Determination of the Barrier Height for Acetyl Radical Dissociation from Acetyl Chloride Photodissociation at 235 nm Using Velocity Map Imaging†

Xiaonan Tang, Britni J. Ratliff, Benjamin L. FitzPatrick, and Laurie J. Butler*

The James Franck Institute and Department of Chemistry, University of Chicago, Chicago, Illinois 60637

Received: June 30, 2008; Revised Manuscript Received: August 15, 2008

This work uses velocity map imaging to determine the barrier height for acetyl radical, CH_3CO, dissociation to $CH_3 + CO$. Photodissociation of acetyl chloride at 235 nm generates acetyl radicals with an internal energy distribution spanning this barrier. We determine the velocity and internal energy distribution of all nascent acetyl radicals, stable and unstable, by measuring the velocities of the $Cl(^2P_{3/2})$ and $Cl(^2P_{1/2})$ cofragments. These Cl cofragments are detected with $2 + 1$ resonance-enhanced multiphoton ionization (REMPI) in a spin−orbit branching ratio $Cl(^2P_{3/2})$:$Cl(^2P_{1/2})$ of 3.3 ± 0.2. Using 157 nm photoionization, we then detect the recoil velocities of the energetically stable acetyl radicals. The radicals and momentum matched Cl atoms evidence parallel angular distributions. Comparison of the total recoil translational energy distribution $P(E_T)$ for all radicals to that obtained from the detection of stable radicals yields an onset for dissociation at a translational energy of 25.0 ± 0.4 kcal/mol. From this onset we can calculate the barrier height for $CH_3CO \rightarrow CH_3 + CO$, but this relies on prior determinations of the C−Cl bond energy of acetyl chloride. Using an experimental bond dissociation energy of 83.4 ± 0.2 kcal/mol yields a dissociation barrier of 14.2 ± 0.5 kcal/mol. Our data evidence that a portion of the acetyl radicals formed with total internal energy above the barrier are stable due to the partitioning of energy into rotation during the C−Cl bond fission of the precursor. Thus, the internal energy onset for dissociation is not as sharp as was assumed in prior determinations of the barrier. The experimentally determined onset is compared with that predicted from electronic structure calculations at the G3//B3LYP and CCSD(T) levels of theory.

I. Introduction

Numerous groups have studied the photodissociation dynamics of acetyl chloride[1−6] and the unimolecular decomposition reaction dynamics of the acetyl radical, CH_3CO.[5−11] The photodissociation of acetyl chloride at 248 nm occurs via a $^1[n_O, \pi^*_{C=O}]$ excitation and results in the breaking of the C−Cl bond rather than the C−C bond.[2,6] The angular distribution of the Cl and CH_3CO photofragments is anisotropic with β values reported between 0.9−1.0.[1,6,7,10] This fast α-bond cleavage indicates that the dissociation occurs adiabatically on a singlet A″ electronic state rather than undergoing intersystem crossing to the triplet state.[1,8]

Numerous experimental and computed barrier heights[5−7,9,10,12−14] for this dissociation channel have been published with values ranging widely from 11.1 to 21.1 kcal/mol. A summary of select recent values are listed in Tables 1 and 2. Some of these experiments measured a kinetic energy threshold for CH_3CO radicals produced photolytically from acetyl chloride, so their barrier height determinations rely on an assumed value for the C−Cl bond dissociation energy. For comparison with the present work, Table 1 recalculates the reported barriers in prior work using an updated experimental dissociation energy of 83.4 ± 0.2 kcal/mol for the C−Cl bond energy calculated from the heats of formation[15−17] at 298 K and the appropriate enthalpy increments needed to adjust these values to 0 K.[16,18] We also use a different assumption regarding the internal energy of the photolytic precursor.

Using photofragment translational spectroscopy, North et al.[5,6] report two measurements of the acetyl dissociation barrier height, one using acetyl chloride and the other using acetone as the photolytic precursors. Their data show that the acetyl radicals produced in the lower recoil kinetic energy photolysis events are lost due to their high internal energy and resulting secondary dissociation to $CH_3 + CO$. Thus they derive a barrier for the secondary dissociation process from the experimentally determined kinetic energy threshold for loss of acetyl radicals. In their analysis, however, they assume that the recoil kinetic energy distribution, $P(E_T)$, used to fit the stable acetyl product is sharply truncated at the observed threshold. Though this gives a good fit to their data, their analysis assumes that all radicals with internal energy above the threshold dissociate, not accounting for the fact that some of the available energy may be partitioned into rotational energy of the radical or into spin−orbit excitation of the Cl cofragment. Radicals formed in conjunction with spin−orbit excited $Cl(^2P_{1/2})$ have 2.52 kcal/mol less internal energy at a given recoil kinetic energy, thereby causing them to have a higher E_T threshold than radicals formed in conjunction with $Cl(^2P_{3/2})$. They also assume the internal energy of the acetyl radical precursor is substantially cooled in the supersonic expansion. We analyze these effects further in this paper.

Subsequent work by Suzuki and co-workers[10] sought to time resolve the unimolecular dissociation of acetyl radicals produced from the photolysis of acetyl chloride. Interestingly, when they binned the acetyl radicals by recoil velocity, and thus crudely by internal energy, they found the measured dissociation rates were markedly slower than those predicted by statistical theories. Again, they did not account for the possibility that significant rotational energy is imparted to the acetyl radical during photolysis. However, their experiments do offer a firm upper bound on the $CH_3 + CO$ dissociation barrier. About a quarter

† Part of the "Karl Freed Festschrift".

* Corresponding author. E-mail: L-Butler@uchicago.edu.

10.1021/jp8057417 CCC: $40.75
Published on Web 10/31/2008

TABLE 1: Select Experimental Measurements of the Barrier Height for Acetyl Radical Dissociation to $CH_3 + CO$

experimental method	λ (nm)	threshold E_T (kcal/mol)	reported barrier (kcal/mol)	recalculated barrier[a]
photofragment translational spectroscopy[b]	248	15.0	17 ± 1	18.2 ± 1[c]
photofragment translational spectroscopy[d]	248	13.5	17.8 ± 3	
kinetic measurement[e]			$E_a = 17.2 \pm 0.5$	
subpicosecond time clocked photofragment imaging[f]	255		$\leq 17 \pm 1$	$\leq 17.7 \pm 1$[g]
velocity map imaging (this work)	235	25.0 ± 0.4	14.2 ± 0.5	14.2 ± 0.5

[a] Values recalculated by accounting for the thermal vibrational energy in the precursor and using the updated[16b] experimental C−Cl bond energy of 83.41 kcal/mol. The updated experimental bond energy is 0.19 kcal/mol lower[16b] than the best prior value of 83.6 kcal/mol. The prior value was calculated using the $\Delta H_f^\circ(CH_3COCl)$ at 298 K of -58.03 ± 0.2 kcal/mol,[15] an ATcT value of -2.48 ± 0.21 kcal/mol at 298 K for CH_3CO,[15b,16b] and $\Delta H_f^\circ(Cl)$ at 298 K of 28.992 kcal/mol.[16a,17] The enthalpies of formation at 298 K were then corrected to 0 K values using enthalpy increments for CH_3CO of 2.984 kcal/mol,[15b,16b] Cl of 1.499 kcal/mol,[16a,b] and gaseous CH_3COCl of 3.529 kcal/mol.[18] [b] From the work of North et al.[5] [c] The nozzle temperature was 353 K giving $\langle E_{vib}(CH_3COCl)\rangle = 1.6$ kcal/mol. [d] From the work of North et al.[6] This work used acetone as the photolytic precursor and $D_o(C-Cl) = 83.7$ kcal/mol. [e] From the work of Watkins and Word.[9] [f] From the work of Shibata et al.[10] [g] The reported work did not give the nozzle temperature, so we assume it to be 298 K giving $\langle E_{vib}(CH_3COCl)\rangle = 1.1$ kcal/mol.

TABLE 2: Select Theoretical Predictions of the Barrier Height for Acetyl Radical Dissociation to $CH_3 + CO$

theoretical method	barrier[a] (kcal/ mol)
MP2/cc-pVTZ[b]	18.7
G2//G2Q[c]	17.3
MP2/6-31 g(d)[d]	18.5
G3//B3LYP/6-31 g(d)[e]	15.2
G3//B3LYP/6-311 g(d,p)[f]	15.6
G3//B3LYP/6-311++g(d,p)[f]	15.73
CCSD(T)[f]	16.77

[a] Including zero-point corrections. [b] From the work of Deshmukh et al.[7] [c] From the work of Osborn et al.[12] [d] From the work of Liu et al.[13] [e] From the work of Miller et al.[14] [f] This work.

of the CH_3CO acetyl radicals formed in the lowest internal energy range (this is reported as 16−18 kcal/mol for acetyl radicals formed in conjunction with $Cl(^2P_{3/2})$, assuming $D_0(C-Cl) = 83$ kcal/mol and the internal energy of the photolytic precursor is zero) dissociate after 600 fs. Thus, they report an upper limit of 17 ± 1 kcal/mol for the $CH_3CO \rightarrow CH_3 + CO$ barrier. Finally Watkins and Word[9] performed a kinetics experiment on the addition of methyl radicals to carbon monoxide which included an elementary step involving the decomposition of acetyl radicals. Their analysis derived an activation energy of 17.2 kcal/mol ± 0.5 kcal/mol at 298 K.

In this study we obtain a more accurate measurement of the barrier height for acetyl radical dissociation to CH_3+ CO and resolve the distribution of acetyl radicals that are stable despite having a total internal energy above the barrier. The method is similar to that of our earlier work on determining the barrier for acrolyl radical decomposition.[19] The photodissociation of acetyl chloride at 235 nm produces acetyl radicals spanning the range of theoretical and experimental barriers for the dissociation of CH_3CO to $CH_3 + CO$. Using [2 + 1] REMPI, the Cl atoms in each spin−orbit state, $Cl(^2P_{3/2})$ and $Cl(^2P_{1/2})$, are selectively ionized and detected. Using momentum conservation, the total recoil translational energy distribution from photodissociation is obtained from the detection of the Cl photofragments. One expects the dissociation lifetime of acetyl radicals formed with vibrational energy even 0.1 kcal/mol above the dissociation barrier to be short; so only acetyl radicals with vibrational energy below the barrier are detected. Since the $P(E_T)$ obtained from the nascent Cl products is the recoil kinetic energy distribution of Cl recoiling from both stable and unstable acetyl radicals, comparison with the energy distribution obtained from the detection of stable CH_3CO radicals reveals the recoil kinetic energy threshold for producing unstable radicals. In this way we directly measure the barrier height for CH_3CO dissociation to $CH_3 + CO$.

II. Experimental Methods

A. Velocity Map Imaging. This experimental setup has been previously described in detail,[20−24] so only a brief outline will be provided here. A 10% molecular beam was created by bubbling helium gas through a cooled liquid sample of acetyl chloride (Aldrich, 98%) at −20 °C. At a total stagnation pressure of 550 Torr, the molecular beam was supersonically expanded through a room temperature pulsed valve with an orifice diameter of 0.8 mm into the photodissociation region via a skimmer. The parent molecules in the long (∼300 μs) stable region of the expansion were photodissociated with a focused 235 nm beam generated by tripling the output of a Lamda Physik FL 3002 dye laser pumped by the second harmonic of a Nd: YAG laser operating at 21 Hz. Using 2 + 1 REMPI, the $Cl(^2P_{3/2})$ or $Cl(^2P_{1/2})$ fragments were selectively ionized by scanning the Doppler profiles centered at 235.33 nm ($4p\ ^2D_{3/2} \leftarrow 3p\ ^2P_{3/2}$) or 235.20 nm ($4p\ ^2P_{1/2} \leftarrow 3p\ ^2P_{1/2}$), respectively.[24] The laser power was reduced to render Coulomb repulsion between the ions insignificant. The acetyl radicals were ionized with a 157 nm beam generated from a GAM (EX10F/ 300) F_2 laser which was fired 40 ns after the photolysis laser. RRKM calculations indicate that CH_3CO radicals with energy 0.1 kcal/mol above the barrier have a lifetime of $\approx 5 \times 10^{-10}$ s.[8] As predicted by the short lifetime of the radical, the magnitude of this delay was found to have negligible effect on the radical signal when varied between 10 and 400 ns. The path of the 157 nm beam was evacuated to minimize the absorption by O_2 and N_2 en route to the high vacuum chamber. The electrostatic lens optics with a repeller voltage of 2000 V and extractor voltage of 1424 V accelerated the spherically expanding ions down a ∼577 mm grounded time-of-flight tube toward the detector. The detector consisted of a position sensitive Chevron microchannel plate assembly (MCP) coupled to a P20 phosphor screen. The voltage of the front plate of the MCP was pulsed to −750 V for 80 ns to mass selectively detect ions based on their arrival time. The phosphor screen was maintained at 3.3 kV above the potential of the rear MCP plate. A cooled charge-coupled device (CCD) camera with a standard 35 mm lens was used to grab images of the ions and store them in the

computer using the ion-counting method.[25] The resolution of the image is $\Delta v/v = 0.048$ at 1153 m/s and 0.036 at 1450 m/s when calibrated with O_2. The raw images were symmetrized about the vertical and horizontal axes in the data analysis.

B. Theoretical Methods. Calculations of the C−Cl bond energy for acetyl chloride and the transition state for acetyl radicals dissociation were performed at both G3//B3LYP/6-311++G(d,p) and UCCSD(T)/CBS//UCCSD(T)/aug-cc-pVTZ levels of theory, where CBS stands for complete basis set. For the G3//B3LYP results, we used the Gaussian 03 program, revision E.01.[26] Optimized molecular geometries and vibrational frequencies were found using the B3LYP density functional with the 6-311++G(d,p) basis set. The geometries were converged to a root-mean-square (rms) force below 1×10^{-6} and an rms displacement below 4×10^{-6}, where both are in atomic units. The G3//B3LYP calculations[27] were performed on B3LYP/6-311++G(d,p) optimized geometries. To compute the zero-point vibrational energies, the B3LYP vibrational frequencies were scaled by 0.96 as recommended by Scott and Radom[28] and required by the G3//B3LYP method. Wave functions for doublet species were spin-unrestricted, and wave functions for singlet species were spin-restricted. The transition-state structure was confirmed by having only one imaginary frequency with motion along the reaction coordinate. An intrinsic reaction coordinate (IRC) calculation was performed as an additional check. All energies are presented as zero-point corrected enthalpies of formation at zero Kelvin.

The coupled cluster geometry optimizations and single-point calculations were performed with MOLPRO[29] using a UCCSD(T)[30]/aug-cc-pVTZ[31] with an ROHF reference. On advice,[32] we chose unrestricted open-shell coupled cluster instead of restricted open-shell and checked that the spin contamination was minimal. No symmetry was assumed and multiple optimizations were carried out (e.g., $CH_3CO(Cl)$ was optimized having either O or Cl staggered with respect to the hydrogen atoms on the methyl group) in order to find the structures corresponding to the global minima. Again, the geometries converged to a root-mean-square (rms) force below 1×10^{-6} and an rms displacement below 4×10^{-6}, where both are in atomic units. Intrinsic reaction coordinate calculations were performed at the UCCSD(T)/aug-cc-pVDZ level of theory for the transition state to make sure it corresponds to the correct reactant and product wells. Single-point frozen-core UCCSD(T)[30] energies were calculated using the augmented correlation-consistent basis sets (fragments containing chlorine atoms utilized the updated aug-cc-pV(N+d)z basis sets[33] containing an additional tight d function), and ROHF and correlation energies were converged to less than one microhartree. A two-point CBS extrapolation devised by Helgaker[34] was applied independently to the singles and doubles correlation energy (CCSD - ROHF) and to the triples energy using quadruple- and 5-ζ basis set results. The reference energies utilized the 6-ζ basis set and were not extrapolated. We accounted for core-valence correlation by extrapolating the differences between two all-electron calculations (using the aug-cc-pwCVTZ and aug-cc-pwCVQZ basis sets,[35] with the 1s orbital on chlorine frozen) and the triple- and quadruple-ζ frozen-core calculations. Additionally, we included relativistic effects using sixth-order Douglas-Kroll-Hess (DKH6) calculations with the aug-cc-pV5Z_DK basis sets (chlorine was again augmented with tight d functions),[36] and the correction was taken as the difference between the DKH6 UCCSD(T) energy and the analogous calculation used in the extrapolations. Both of the above basis sets were taken from the EMSL basis set exchange.[37,38] The single-point energies include a zero-point energy (ZPE) correction based on unscaled UCCSD(T)/aug-cc-pVTZ frequencies with anharmonic corrections from MP2/aug-cc-pVTZ for the closed-shell photolytic precursor and UMP2/aug-cc-pVTZ for the open-shell species using the Gaussian 03[26] program. It should be noted that the method for generating the anharmonic corrections is very crude, but it should yield qualitatively accurate corrections at the very least. The spin−orbit energy correction for chlorine was taken from Moore's tables[24] and applied when calculating the bond dissociation energy of the precursor. All of the relevant structures, energies, unscaled vibrational frequencies, anharmonic corrections, and rotational constants of the precursor, CH_3CO and Cl radicals, and transition state leading to $CH_3 + CO$ calculated at the G3//B3LYP/6-311++G(d,p) and UCCSD(T)/CBS//UCCSD(T)/aug-cc-pVTZ levels of theory are given in the Supporting Information.

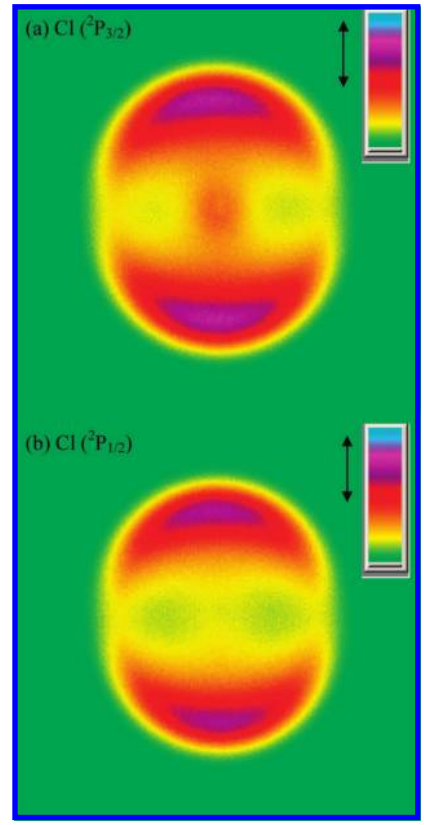

Figure 1. Raw images of (a) Cl($^2P_{3/2}$) obtained with dissociation and probe at a vacuum wavelength of 235.33 nm via the 4p $^2D_{3/2} \leftarrow$ 3p $^2P_{3/2}$ transition; (b) Cl($^2P_{1/2}$) obtained with dissociation and probe at a vacuum wavelength of 235.20 nm via the 4p $^2P_{1/2} \leftarrow$ 3p $^2P_{1/2}$ transition. The laser polarization is along the vertical direction in the plane of the images as shown with the arrows. The image depicted is 901 × 901 pixels with a linear intensity scale shown in the top right corner of each image. The images appear oval in shape due to the parallel angular distribution and speed dependence (see text) of the anisotropy.

III. Results

A. Recoil Translational Energy Distribution from Acetyl Chloride Photodissociation. The total recoil translational energy distribution for C−Cl bond fission from the 235 nm photodissociation of acetyl chloride, generating both energetically stable and unstable radicals, is determined by detecting the Cl cofragments. Ion images of the ^{35}Cl($^2P_{1/2}$) and ^{35}Cl($^2P_{3/2}$) photofragments are shown in Figure 1 with the laser polarization along the vertical axis. Each image is used to reconstruct a three-dimensional scattering distribution using an

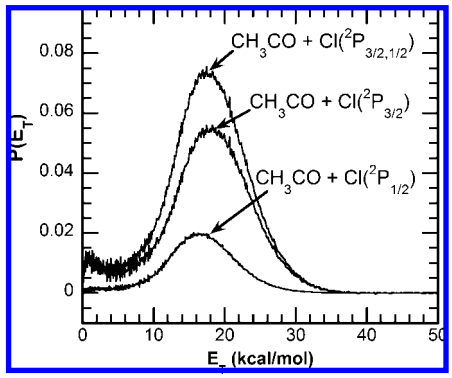

Figure 2. Normalized total $CH_3CO + Cl$ ($^2P_{1/2,\ 3/2}$) center-of-mass recoil translational energy distribution. This total $P(E_T)$, resulting in both stable and unstable acetyl radicals, is a sum of the $Cl(^2P_{3/2})$ and $Cl(^2P_{1/2})$ distributions determined from the images in Figure 1. These distributions were baseline corrected to oscillate around zero from 40−52 kcal/mol and weighted by their spin−orbit branching ratio of 3.3 ± 0.2.

inverse Abel transformation.[39] The speed distributions, $P_{Cl}(v)$, of the Cl fragments are extracted by integrating the three-dimensional velocity distributions over all solid angles at each speed. Using momentum conservation and the appropriate Jacobian, the center of mass recoil translational energy distributions $P(E_T)$ from the photodissociation are derived from the Cl speed distributions. The $P(E_T)$ for the dissociation events forming $Cl(^2P_{3/2})$ evidence a bimodal distribution: a minor low kinetic energy component is apparent and has been noted before,[7] but it is not our focus here. The sum of the kinetic energy distributions calculated from $^{35}Cl(^2P_{3/2})$ and $^{35}Cl(^2P_{1/2})$, weighted by their spin−orbit branching ratio of 3.3 ± 0.2, gives the total recoil kinetic energy distribution shown in Figure 2. We determine the $^{35}Cl(^2P_{3/2})$:$^{35}Cl(^2P_{1/2})$ branching ratio by integrating the total ion signal in images accumulated over the entire Doppler profile and weighting by the REMPI linestrength.[40] The error bars are reported within the 95% confidence interval from 10 trials. Deskmukh et al.[3] reported the spin orbit branching ratio of $Cl(^2P_{3/2})$:$Cl(^2P_{1/2})$ as 1.5.

Photodissociation of acetyl chloride produces radicals momentum matched to both Cl isotopes, so the data is fit accordingly. To confirm our expectation that the total recoil kinetic energy distribution is independent of isotope, we took ion images of $^{37}Cl(^2P_{3/2})$. As expected, the $P_{Cl}(v)$ for the ^{37}Cl data is shifted to slower speeds than the ^{35}Cl velocity distributions, but the resulting recoil kinetic energy distributions are essentially identical to that obtained for ^{35}Cl. All further analysis uses the total kinetic energy distribution obtained from the detection of ^{35}Cl. The observed ^{35}Cl:^{37}Cl signal is roughly 3:1, in accordance with the expected isotopic ratio of 0.7577:0.2423. Figures and data analysis of the ^{37}Cl isotope can be found in the Supporting Information.

B. Internal Energy Comparison of Nascent and Stable Radicals. Using energy conservation, the internal energy, rotational plus vibrational, of the nascent radicals $E_{int}(CH_3CO)$ is calculated from the following equation

$$E_{int}(CH_3CO) = E_{h\nu} + E_{int}(CH_3COCl) - D_0(C-Cl) - E_{int}(Cl(^2P_J)) - E_T \quad (1)$$

where $E_{h\nu}$ is the energy of the photon used for photodissociation, in this case 121.5 kcal/mol. It is assumed that the parent molecules are rotationally cooled and have a thermal distribution of vibrational energy at the nozzle temperature, 298 K. The

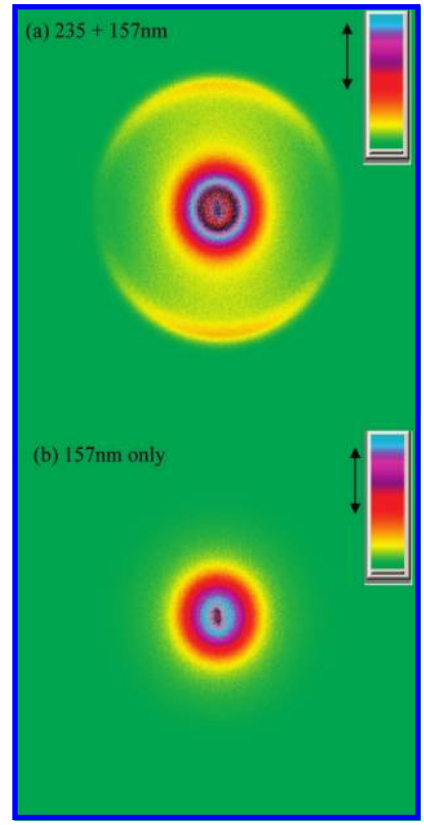

Figure 3. Raw images of the CH_3CO fragments obtained using lasers at (a) 235 + 157 nm and (b) 157 nm. The high-translational energy component appearing in part a but not in part b is from photodissociation of acetyl chloride at 235 nm and ionization at 157 nm. The photolysis laser was polarized in the vertical direction in the plane in the images, as shown by the arrow. The images depicted are 901 × 901 pixels with a linear intensity scale shown in the top right-hand corner of each image.

average internal energy of the precursor, $E_{int}(CH_3COCl)$, is estimated to be 1.1 kcal/mol using the scaled vibrational frequencies calculated at the B3LYP/6-311++G(d,p) level. Vibrational frequencies calculated at the MP2//6-311g(d,p) level also predict 1.1 kcal/mol of internal energy in the precursor. Throughout the results section we use the experimental value of 83.4 ± 0.2 kcal/mol for the C−Cl bond energy, $D_0(C-Cl)$. Comparisons with theoretical predictions are presented in the discussion. The internal energy in each Cl spin−orbit state, $E_{int}(Cl(^2P_{3/2}))$ and $E_{int}(Cl(^2P_{1/2}))$, is 0 and 2.52 kcal/mol, respectively.

Ionization and detection of the acetyl radical cofragments provide a measurement of the internal energy distribution for the portion of nascent radicals that are stable. To obtain the translational energy distribution of the stable portion of the CH_3CO radicals resulting from the photodissociation of acetyl chloride at 235 nm, we ionize the CH_3CO photofragments with 157 nm light. The raw images, Figure 3, show that the signal appearing at the center of the images at low translational energies is background signal due to photodissociation and photoionization with 157 nm; thus, it is strongly dependent upon the excimer laser power. Consistent background subtraction is difficult, but fortunately, the 157 nm background signal has little contribution in the high kinetic energy region. Thus, we scale the translational energy distribution from 157 nm photodissociation so that the baseline signal oscillates around zero from v = 1835−2360 m/s. The plots of this analysis are in the Supporting Information. Since 235 nm photons do not have

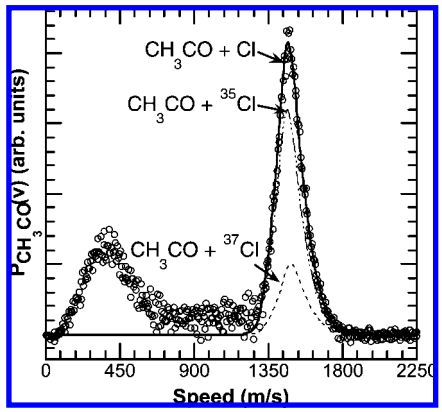

Figure 4. $P(v)$ distribution for the acetyl radical produced from 235 nm photodissociation of acetyl chloride and 157 nm photoionization. The experimental data are shown as solid circles, and the forward convolution fit (solid line) is calculated from the total recoil translational energy distribution in Figure 5 by assuming 75.78% of the acetyl radicals recoil from ^{35}Cl (dot-dashed line) and 24.22% of the acetyl radicals recoil from ^{37}Cl (dashed line), in accordance with the isotopic ratio.

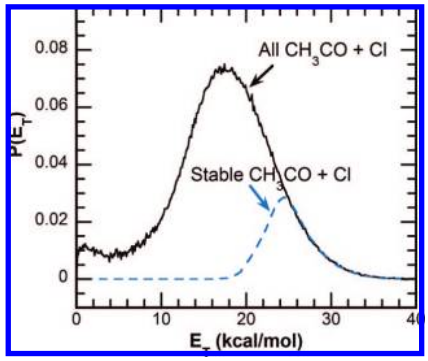

Figure 5. Center of mass translational energy distributions for the C−Cl bond fission of acetyl chloride. The total recoil kinetic energy, shown as the solid line, results in both stable and unstable radicals; it is derived from the Cl data. The portion of this distribution that results in stable radicals is shown as the dashed line; it was obtained from the forward convolution fit to the measured speed distribution of the detected CH_3CO radicals as described in the text.

enough energy to ionize the acetyl radical, there is no observed background signal from only the 235 nm beam.

To derive the translational energy distribution for the detected acetyl radicals, a forward convolution method was used. The acetyl radicals in the image result from the dissociation of acetyl chloride to yield acetyl radicals recoiling from both ^{35}Cl and ^{37}Cl. The Cl data show that the $P(E_T)$ for these two processes are identical. We iteratively adjust a total recoil kinetic energy distribution for stable acetyl radicals $P(E_T)$ until a good fit to the measured acetyl radical $P_{CH_3}CO(v)$ is achieved. The predicted fit, $P_{CH_3}CO(v)$, is a sum of the speed distributions of the radicals recoiling from each Cl isotope, derived from the assumed $P(E_T)$ and weighted by the Cl isotopic ratio. The forward convolution fit, derived from the $P(E_T)$ shown as the dashed line in Figure 5, is superimposed on the experimental speed distribution in Figure 4.

Figure 5 directly compares the total recoil kinetic energy distribution derived from the Cl atom data, representing all C−Cl bond fission events, with the recoil kinetic energy distribution for the photodissociation events producing stable acetyl radicals. For high recoil kinetic energy events producing low internal energy radicals, all radicals are formed below the dissociation barrier so the two $P(E_T)$s depicted in Figure 5 are

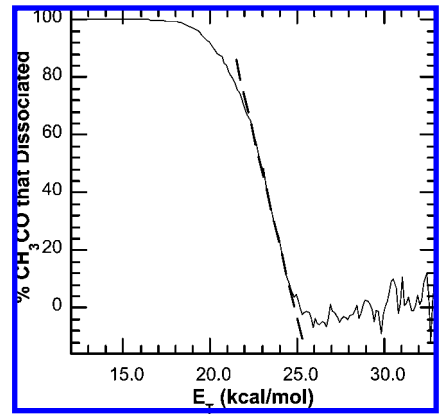

Figure 6. Percent of dissociated radicals as a function of CH_3CO + Cl recoil kinetic energy (solid line). The x-intercept of the linear fit (dashed line) of the data between 23.5 and 24.5 kcal/mol was used to determine 25.0 ± 0.4 kcal/mol as the threshold E_T for acetyl dissociation.

identical. At the kinetic energy threshold of 25 kcal/mol, the distribution derived from the stable acetyl radical spectra falls below the total $P(E_T)$ for producing both stable and unstable radicals. Interestingly, the data show that a substantial portion of the radicals remain stable at recoil kinetic energies lower than this threshold energy; the truncation is not sharp as assumed in the prior work of North et al.[5]

Figure 6 shows the percent of dissociated radicals as a function of translational energy. A linear fit to the data between 23.5−24.5 kcal/mol reveals a kinetic energy threshold of 25.0 ± 0.4 kcal/mol. The error bars represent the 95% confidence interval from four independent sets of data. Notice that stable acetyl radicals are detected even at 6 kcal/mol below the threshold kinetic energy. Radicals formed in conjunction with Cl($^2P_{1/2}$) would have a threshold kinetic energy at 22.48 kcal/mol, so the observation of stable acetyl radicals at even lower kinetic energies suggests that significant energy is partitioned to rotational energy for some of the acetyl radicals. We return to this point in the discussion.

C. Deriving the Barrier Height for CH_3CO Dissociation. The internal energy distribution of stable radicals is derived from our measured $P(E_T)$ using eq 1. Note that North[5,6] and Suzuki[10] assumed the internal energy of the precursor was zero when they determined a barrier height for their data, so when comparing to their work in Table 1, we recalculated their derived barrier in the last column. A plot of the measured internal energy distributions of all nascent radicals + Cl atoms (determined from the Cl atom data) is shown in Figure 7 superimposed on the potential energy surface calculated at the G3//B3LYP/6-311++G(d,p) level. The figure also shows the distribution corresponding to stable radicals + Cl detected in our image of CH_3CO^+. At low internal energy, the two distributions are identical as these radicals do not have sufficient internal energy to dissociate. However, as the internal energy of the radical increases and surpasses the dissociation barrier height, the two distributions diverge. Clearly, at the threshold recoil kinetic energy the dissociative radicals would be produced in coincidence with Cl($^2P_{3/2}$) atoms, as radicals produced in coincidence with Cl($^2P_{1/2}$) with the same recoil kinetic energy would have a 2.52 kcal/mol less internal energy and would be still stable. Using our kinetic energy threshold of 25.0 ± 0.4 kcal/mol with an experimental bond dissociation energy of 83.4 ± 0.2 kcal/mol yields a derived dissociation barrier of 14.2 ± 0.5 kcal/mol. The error bars propagate the uncertainty in the experimental bond dissociation energy and kinetic energy threshold but do

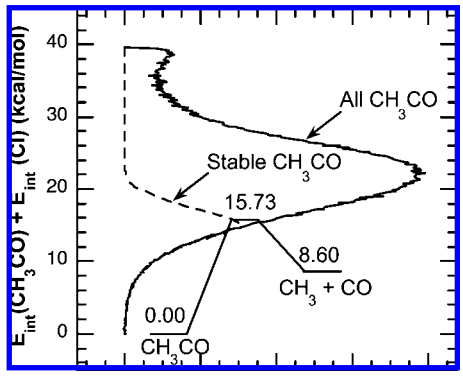

Figure 7. Measured internal energy distribution (solid line) of all the nascent radicals + Cl atoms (determined from the Cl atom data) is superimposed on the potential energy surface calculated at the G3// B3LYP/6-311++G(d,p) level. The distribution corresponding to stable radicals + Cl is also shown (dashed line).

not account for the uncertainty in the internal energy of the photolytic precursor. We compare these results to two theoretical predictions in the discussion.

D. Dynamics of Acetyl Chloride Photodissociation. The linear polarization of the photolysis laser allows for the study of the angular distribution[41−44] of acetyl chloride photodissociation at 235 nm. The recoil angular distributions are shown in Figure 8. The $Cl(^2P_{3/2})$ angular distribution is fit using

$$I(\theta) \propto 1 + \beta_2 P_2(\cos\theta) + \beta_4 P_4(\cos\theta) \quad (2)$$

as the signal depends both on the anisotropy of the photodissociation process and on the REMPI detection of the $J = {}^3/_2$ atoms. The $Cl(^2P_{1/2})$ and CH_3CO angular distributions are fit with

$$I(\theta) \propto \frac{1}{4\pi}[1 + \beta P_2(\cos\theta)] \quad (3)$$

where θ is the angle between the recoiling fragment's velocity vector and the electric vector of the photolysis laser. β is the anisotropy parameter, P_2 is the second-order Legendre polynomial, and P_4 is the fourth-order Legendre polynomial.

We examine the anisotropy of two kinetic energy ranges which correspond roughly to the formation of unstable versus stable radicals. The signal appearing in the Cl images in the range of 200−275 pixels from the center of the image corresponds to a recoil kinetic energy range (for vertically recoiling fragments) of 10.3−19.5 kcal/mol. This is the range in which momentum matched radicals are unstable. In this range, the $\beta_2 = 1.00 \pm 0.07$ and $\beta_4 = -0.04 \pm 0.01$ for $Cl(^2P_{3/2})$ while $\beta = 1.01 \pm 0.01$ for $Cl(^2P_{1/2})$. As the recoil kinetic energy increases, the radicals are formed with decreasing internal energy. Thus, the signal appearing in the Cl images in the range of 275−350 pixels from the center of the image, which corresponds to a vertical recoil kinetic energy range of 19.5−31.6 kcal/mol, is due primarily to stable radicals. In this higher kinetic energy range, $Cl(^2P_{3/2})$ atoms recoil with anisotropy $\beta_2 = 1.32 \pm 0.11$ and $\beta_4 = 0.10 \pm 0.02$ while $Cl(^2P_{1/2})$ atoms have β of 1.34 ± 0.03. The anisotropy of the Cl atoms increases gradually as a function of recoil kinetic energy. These anisotropy parameters confirm previous results indicating that the dissociation of acetyl chloride is prompt relative to molecular rotation and that the transition is predominantly parallel.

On the basis of momentum conservation, the angular distribution of the CH_3CO radicals should be an average of the anisotropies from the two spin−orbit Cl cofragments in the high-velocity portion of the distribution, weighted by the experimentally determined spin−orbit branching ratio. Since β_4 is essentially 0, we calculate the expected anisotropy of the acetyl radical to be 1.33 ± 0.03. Integrating the CH_3CO signal over the pixel range of 250−315, which corresponds to a maximum vertical recoiling energy of 19.8−31.4 kcal/mol, we find the CH_3CO anisotropy parameter β of 1.35 ± 0.03. The polarization of the 157 nm probe light in the plane perpendicular to the 235 nm beam and the molecular beam does not seem to significantly affect the anisotropy measurement. Plots of the angular distribution for the higher kinetic energy range are shown in Figure 8. All error bars are reported within the 95% confidence interval using results from four trials. These experimental results are within reasonable agreement with previously published results.[1,7,8,10]

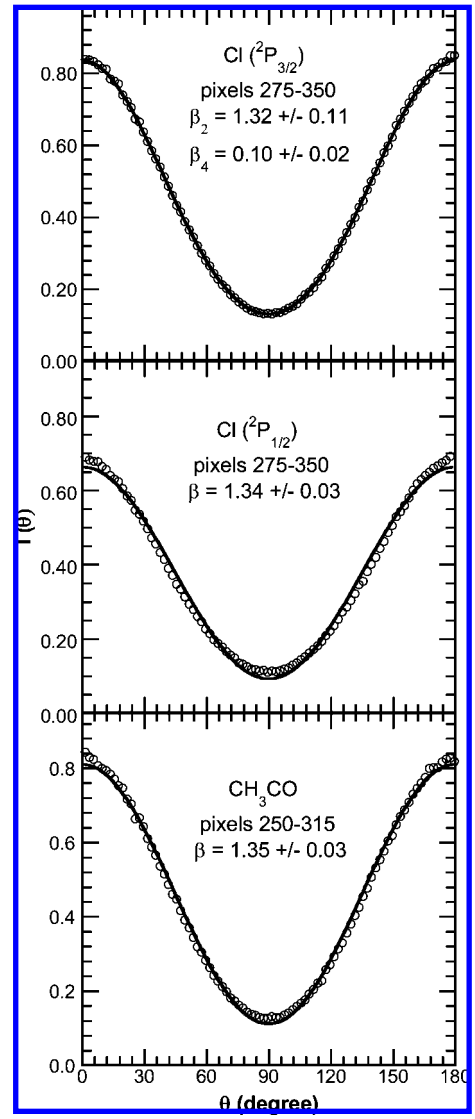

Figure 8. Angular distributions for $Cl(^2P_{3/2})$, $Cl(^2P_{1/2})$, and CH_3CO. Raw data is shown as open circles, and the fit is shown as a solid line.

IV. Discussion

To compare the best prior measurement, that by North, et al.,[5] of the $CH_3CO \rightarrow CH_3 + CO$ barrier to the present determination, we first note that North's analysis assumed the internal energy of the acetyl chloride precursor was effectively cooled in the supersonic expansion. However, North's data was taken with a continuous beam of acetyl chloride seeded in helium at a very low stagnation pressure, P_0, of 50 Torr and

small nozzle diameter d (P_0d = 18.5 Torr-mm). For such a modest expansion in helium one can expect substantial cooling in the rotational degrees of freedom but not in the vibrational degrees of freedom. In our analysis, we assume the following compromise: the rotational degrees of freedom are completely cooled and the vibrational degrees of freedom are not cooled. Because the barrier is determined from a threshold measurement, if a portion of the precursors are vibrationally hot the threshold would reflect the radicals formed from the hotter precursors. Thus, correcting North's barrier determination to account for the 1.6 kcal/mol of vibrational energy in their uncooled precursors (at a nozzle temperature of 80 °C) and the 0.41 kcal/mol update to the bond energy, the barrier determined from their data would have been reported as 18.2 kcal/mol as opposed to 17 kcal/mol. Note this barrier determination is substantially larger than ours.

The present data allows us to determine a more accurate barrier height for the dissociation of the acetyl radical to CH_3 + CO because we were able to resolve two other features of the data. Previous experiments by North and co-workers[5] were unable to measure the Cl atom spin−orbit distributions and assumed the energy imparted into rotation of the radical was negligible and therefore fit their data with a sharply truncated $P(E_T)$. While North's[5] primary data is roughly consistent with ours, we are able to resolve the production of $Cl(^2P_{3/2})$ vs Cl ($^2P_{1/2}$) and we have the resolution needed to detect the distribution of radicals below the kinetic energy threshold which are stable due to their rotational energy. As expected, this resolution shifts our threshold kinetic energy higher and thus decreases our derived barrier height. The radicals detected at kinetic energies below our threshold kinetic energy result only in a small part because some radicals are produced in conjunction with excited-state Cl. It is clear that there is rotational excitation in the acetyl radical because this region is much wider than 2.52 kcal/mol. While the impact parameter for the dissociation of acetyl chloride is small (≈0.1 Å) if one assumes it ensues from the ground-state geometry, it is well-known that n_O, π^* excitation promotes the molecule to an excited state that is pyramidal about the carbonyl carbon. Indeed, crude excited-state calculations[2] suggest that the TS on the excited state is pyramidal, resulting in a larger impact parameter which would impart significant rotational energy[45] to the acetyl radicals. Our data evidence the production of some stable acetyl radicals at recoil kinetic energies extending 6 kcal/mol below the kinetic energy threshold. Thus North's barrier of 17 kcal/mol (corrected to 18.19 kcal/mol as described herein) must be an overestimate as it used a sharply truncated kinetic energy threshold.

The energy imparted to rotation in the photodissociation of acetyl chloride also affects the analysis of Suzuki and co-workers.[10] Suzuki's RRKM rates assumed all internal energy is partitioned to vibrational degrees of freedom of the radical. They noted that the calculated rates are much faster than those experimentally observed. One possible reason for the discrepancy between the measured unimolecular dissociation rate of Suzuki and their RRKM estimates may be that they neglected to account for some of the internal energy of the acetyl radical being partitioned into rotational energy. This would, of course, result in their predicted RRKM rates being too fast.

Our experimental barrier height is directly dependent on the C−Cl bond dissociation energy of the precursor. The experimentally determined E_T cutoff was 25.0 ± 0.4 kcal/mol and, using the best experimental bond energy, we obtained a dissociation barrier height of 14.2 ± 0.5 kcal/mol. Because all of the most accurate experimental determinations of the barrier, including ours, rely on an assumed C−Cl bond energy, we should compare the experimental results with different levels of electronic structure theory by summing the theoretical barrier energy for decomposition, $E_{barrier}(CH_3CO)$, and the theoretically predicted C−Cl bond energy of the precursor.

$$E_{barrier}(CH_3CO) + D_0(C-Cl) = E_{h\nu} + E_{int}(CH_3COCl) - E_{int}(Cl(^2P_{3/2})) - E_{T,threshold} \quad (4)$$

On the right side of eq 4, the experimental kinetic energy threshold, $E_{T,threshold}$, and the other experimental parameters have been described in the results and analysis sections. Our data and analysis thus determine that the sum of the precursor C−Cl bond energy and the acetyl decomposition barrier is 97.6 kcal/mol. Comparing this to an electronic structure prediction at the G3//B3LYP/6-311++G(d,p) level of theory, we sum the theoretically predicted $E_{barrier}(CH_3CO)$ = 15.73 kcal/mol and $D_0(C-Cl)$ = 83.01 kcal/mol and obtain 98.74 kcal/mol. As the estimated uncertainty in each is ∼1 kcal/mol, the prediction is in agreement with the experimental results. In contrast, a very high level ab initio prediction at the CCSD(T) level of theory does not agree as well with the experimental result. The ab initio CCSD(T) prediction for the C−Cl bond energy described at length in the theoretical methods subsection is 83.42 kcal/mol while the acetyl dissociation barrier is predicted to be 16.77 kcal/mol. The sum 100.19 kcal/mol is somewhat larger than the experimental sum of 97.6 kcal/mol. This discrepancy does not appear to be caused by the bond dissociation energy of 83.42 kcal/mol, which is in fortuitously excellent agreement with the experimental value, but it may be in part due to the ad hoc nature of the anharmonic correction that is quite large for the barrier height estimate. The difference may also reflect the difficulty of calculating an accurate $CH_3CO \rightarrow CH_3 + CO$ transition-state energy. The possible multireference nature at the transition state is yet to be investigated. We hope that these new experimental results will stimulate further consideration of these comparisons.

The CCSD(T) calculations presented here include three corrections which are worth analyzing further: an anharmonic correction to the zero-point energy, a core-valence correlation correction, and a relativistic correction. The contribution of each improvement is listed in Table 3. An initial assessment shows that most of the corrections decrease the bond dissociation energy/barrier height, except for the complete basis set extrapolation and the core-valence correlation corrections. This sign difference sets up a delicate interplay between the various corrections. While the magnitude of some entries, such as the large ZPE term, is unsurprising, others are not intuitively obvious when comparing the relative contribution to the bond dissociation energy versus the barrier height. Namely, the anharmonic contribution to the ZPE is miniscule for the bond dissociation energy, but it is sizable for the barrier height, at 0.15 kcal/mol. A second example arises from the core−valence correlation and relativistic corrections. They are relatively small for the bond dissociation energy and almost cancel out one another, but in the case of the barrier height the core−valence correlation correction is four times larger than the relativistic correction. Hence, the net result from the core−valence correlation and relativistic corrections is approximately 0.33 kcal/mol, constituting a sizable adjustment. In contrast, the complete basis set extrapolation makes a sizable correction of almost 0.6 kcal/mol to the bond dissociation energy, but the corresponding correction for the barrier height is much less. It should be noted that an alternate extrapolation scheme, where the entirety of the correlation was extrapolated, was also investigated, and it

TABLE 3: Summary of Corrections Made to CCSD(T) Calculations (in kcal/mol)

energy or correction	D_e[a]	TS_e[a]
E(initial)[b]	86.27	19.36
ΔE(CBS)[c]	0.58	0.15
ΔE(ZPE)[d]	−2.61	−3.21
ΔE(anharmonic)[e]	0.007	−0.148
ΔE(spin−orbit)[f]	−0.84	−
ΔE(core−valence)[g]	0.21	0.44
ΔE(relativistic)[h]	−0.20	−0.11
ΔE(sum)[i]	−2.85	−2.58
E(corrected)[j]	83.42	16.77
ΔE(HLC)[k]	1.37	−

[a] ZPE has intentionally been left out. [b] Reference energy using aug-cc-pV6Z basis and correlation energy using aug-cc-pV5Z. [c] Energy difference between the above scheme and one where the CCSD and (T) energies are extrapolated separately from calculations using the aug-cc-pVQZ and aug-cc-pV5Z bases. [d] Zero-point energy correction using harmonic frequencies from CCSD(T)/aug-cc-pVTZ calculations. [e] Anharmonic correction to the zero-point energy difference using MP2/aug-cc-pVTZ. [f] Spin−orbit correction for Cl as noted in the computational section. [g] Core−valence correlation correction using energy differences extrapolated from aug-cc-pVTZ and aug-cc-pVQZ calculations. [h] Relativistic correction using sixth-order DKH calculations with an aug-cc-pV5Z_DK basis. [i] Sum of the above corrections. [j] Sum of the above value and the value in the first row, E(initial). [k] Using parameter values found in the paper by Baboul, et al.[46]

gave identical results for ΔE(CBS). Table 3 also contains the net result of the higher-level corrections (HLCs) used in the G3 calculations for deriving the bond dissociation energy. As is apparent, the HLC is approximately three times larger than any of the corrections, excluding ZPE and E_{so} because these are explicitly included in G3 as well, used in the coupled-cluster calculations. In summary, accurate bond dissociation energies are affected more by the complete basis set extrapolation than the other, less often used, corrections. The barrier height studied in this system showed less dependence on the complete basis set extrapolation, while anharmonic ZPE corrections and core−valence correlation corrections could play a large role in barrier height accuracy.

Acknowledgment. This work was funded by NSF renewal grant #CHE-0746050 (Butler). B.R. acknowledges the support of an NSF Graduate Research Fellowship. We thank Branko Ruscic for analyzing the primary experimental data on C−Cl bond energies and incorporating that analysis in the Active Thermochemical Tables (ATcT) to obtain a more accurate experimental value. We also thank Kirk Peterson for his illuminating and useful discussions regarding many aspects of the coupled-cluster calculations. Warmest wishes to our wonderful teacher and colleague, Karl Freed.

Supporting Information Available: We provide in the Supporting Information the G3//B3LYP and CCSD(T) results used to calculate the C−Cl bond energy and the $CH_3CO \rightarrow CH_3 + CO$ transition state. These include the structures, energies (with and without a harmonic zero-point correction), vibrational frequencies, and rotational constants. We also provide figures of the $P_{Cl}(v)$ and $P(E_T)$ obtained from data on the mass 35 and 37 $Cl(^2P_{3/2})$ isotopes and also of the 157 nm light background subtraction used when analyzing the CH_3CO data. This material is available free of charge via the Internet at http://pubs.acs.org.

References and Notes

(1) Shibata, T.; Suzuki, T. *Chem. Phys. Lett.* **1996**, *262*, 115.
(2) Sumathi, R.; Chandra, A. K. *J. Chem. Phys.* **1993**, *99*, 6531.
(3) Deshmukh, S.; Hess, W. P. *J. Chem. Phys.* **1994**, *100*, 6429.
(4) Martin, X.; Moreno, M.; Lluch, J. M. *J. Phys. Chem.* **1993**, *97*, 12186.
(5) North, S.; Blank, D. A.; Lee, Y. T. *Chem. Phys. Lett.* **1994**, *224*, 38.
(6) North, S. W.; Blank, D. A.; Gezelter, J. D.; Longfellow, C. A.; Lee, Y. T. *J. Chem. Phys.* **1995**, *102*, 4447.
(7) Deshmukh, S.; Myers, J. D.; Xantheas, S. S.; Hess, W. P. *J. Phys. Chem.* **1994**, *98*, 12535.
(8) Person, M. D.; Kash, P. W.; Butler, L. J. *J. Phys. Chem.* **1992**, *96*, 2021.
(9) Watkins, K. W.; Word, W. W. *Int. J. Chem. Kinet.* **1974**, *6*, 855.
(10) Shibata, T.; Li, H.; Katayanagi, H.; Suzuki, T. *J. Phys. Chem. A* **1998**, *102*, 3643.
(11) Somnitz, H.; Fida, M.; Ufer, T.; Zellner, R. *Phys. Chem. Chem. Phys.* **2005**, *7*, 3342.
(12) Osborn, D. L.; Choi, H.; Mordaunt, D. H.; Bise, R. T.; Neumark, D. M.; Rohlfing, C. M. *J. Chem. Phys.* **1997**, *106*, 3049.
(13) Liu, D.; Fang, W-H.; Fu, X-Y. *Chem. Phys. Lett.* **2000**, *325*, 86.
(14) Miller, J. L.; McCunn, L. R.; Krisch, M. J.; Butler, L. J. *J. Chem. Phys.* **2004**, *121*, 1830.
(15) (a) Pedley, J. B.; Naylor, R. D.; Kirby, S. P. *Thermochemical Data of Organic Compounds*, 2nd ed.; Capman and Hall: London, 1986. (b) Ruscic, B.; Boggs, J. E.; Burcat, A.; Császár, A. G.; Demaison, J.; Janoschek, R.; Martin, J. M. L.; Morton, M. L.; Rossi, M. J.; Stanton, J. F.; Szalay, P. G.; Westmoreland, P. R.; Zabel, F.; Bérces, T. *J. Phys. Chem. Ref. Data* **2005**, *34*, 573–656.
(16) (a) Ruscic, B.; Pinzon, R. E.; Morton, M. L.; von Laszewski, G.; Bittner, S.; Nijsure, S. G.; Amin, K. A.; Minkoff, M.; Wagner, A. F. *J. Phys. Chem. A* **2004**, *108*, 9979–9997. (b) Ruscic, B. Private communication of unpublished interim results from Active Thermochemical Tables (ATcT) ver. 1.37 and the Core (Argonne) Thermochemical Network ver. 1.072 (July 2008). The analysis in ver. 1.37 corrected a potential weak link in the background data supporting the conversion of the experimentally determined enthalpy of hydrolysis of liquid acetyl chloride to the enthalpy of formation of gaseous acetyl chloride. This corrects the prior best value for $D_0(CH_3C(O)-Cl)$ of 83.6 kcal/mol, calculated as described in the footnotes to Table 1, to the current value of 83.41.
(17) Chase, M. W., Jr. NIST-JANAF Thermochemical Tables, 4th edition. *J. Phys. Chem. Ref. Data*, Monograph 9, 1−1951, **1998**.
(18) Overend, J.; Nyquist, R. A.; Evans, J. C.; Potts, J. *Spectrochem. Acta* **1961**, *17*, 1205.
(19) Lau, K.-C.; Liu, Y.; Butler, L. J. *J. Chem. Phys.* **2005**, *123*, 054322.
(20) Heck, A. J. R.; Chandler, D. W. *Annu. Rev. Phys. Chem.* **1995**, *46*, 335.
(21) Eppink, A. T. J. B.; Parker, D. H. *Rev. Sci. Instrum.* **1997**, *68*, 3477.
(22) Sato, Y.; Matsumi, Y.; Kawasaki, M.; Tsukiyama, K.; Bersohn, R. *J. Phys. Chem.* **1995**, *99*, 16307.
(23) Liu, Y.; Butler, L. J. *J. Chem. Phys.* **2004**, *121*, 11016.
(24) Note that most authors label the upper state for detection of $Cl(^2P_{1/2})$ as the $4p\ ^2P_{1/2}$ state from C. E. Moore, "Atomic Energy Levels" NSRDS-NBS 35, 1, 1971. However, the NIST Atomic Spectra Database has adopted the reassignment of this upper state at 85917.937 cm^{-1} to a ^2S state, as recommended in the comprehensive re-analysis of the chlorine spectrum by Radziemski, L. J.; Kaufman, V. *J. Opt. Soc. Am.* **1969**, *59*, 424. To avoid confusion, we give the original C. E. Moore assignment here. For the energy of the transition, we use the NIST value of 85917.937−882.3515 cm^{-1}.
(25) Chang, B.; Hoetzlein, R. C.; Mueller, J. A.; Geiser, J. D.; Houston, P. L. *Rev. Sci. Instrum.* **1998**, *69*, 1665.
(26) Frisch, M. J.; Trucks, G. W.; Schlegel, H. B.; Scuseria, G. E.; Robb, M. A.; Cheeseman, J. R.; Montgomery, J. J. A.; Vreven, T.; Kudin, K. N.; Burant, J. C.; Milliam, J. M.; Iyengar, S. S.; Tomasi, J.; Barone, V.; Mennucci, B.; Cossi, M.; Scalmani, G.; Rega, N.; Petersson, G. A.; Nakatsuji, H.; Hada, M.; Ehara, M.; Toyota, K.; Fukuda, R.; Hasegawa, J.; Ishida, M.; Nakajima, T.; Honda, Y.; Kitao, O.; Nakai, H.; Klene, M.; Li, X.; Knox, J. E.; Hratchian, H. P.; Cross, J. B.; Bakken, V.; Adamo, C.; Jaramillo, J.; Gomperts, R.; Stratmann, R. E.; Yazyev, O.; Austin, A. J.; Cammi, R.; Pomelli, C.; Ochterski, J. W.; Ayala, P. Y.; Morokuma, K.; Voth, G. A.; Salvador, P.; Dannenberg, J. J.; Zakrzewski, V. G.; Dapprich, S.; Daniels, A. D.; Strain, M. C.; Farkas, O.; Malick, D. K.; Rabuck, A. D.; Raghavachari, K.; Foresman, J. B.; Ortiz, J. V.; Cui, Q.; Baboul, A. G.; Clifford, S.; Cioslowski, J.; Stefanov, B. B.; Liu, G.; Liashenko, A.; Piskorz, P.; Komaromi, I.; Martin, R. L.; Fox, D. J.; Keith, T.; Al-Laham, M. A.; Peng, C. Y.; Nanayakkara, A.; Challacombe, M.; Gill, P. M. W.; Johnson, B.; Chen, W.; Wong, M. W.; Gonzalez, C.; Pople, J. A. *Gaussian 03, Revision E.01*; Gaussian, Inc.: Wallingford, CT, 2004.
(27) Baboul, A. G.; Curtiss, L. A.; Redfern, P. C.; Raghavachari, K. *J. Chem. Phys.* **1999**, *110*, 7650.
(28) Scott, A. P.; Radom, L. *J. Phys. Chem.* **1996**, *100*, 16502.
(29) Werner, H.-J.; Knowles, P. J.; Lindh, R.; Manby, F. R.; Schütz, M.; Celani, P.; Korona, T.; Rauhut, G.; Amos, R. D.; Bernhardsson, A.;

Berning, A.; Cooper, D. L.; Deegan, M. J. O.; Dobbyn, A. J.; Eckert, F.; Hampel, C.; Hetzer, G.; Lloyd, A. W.; McNicholas, S. J.; Meyer, W.; Mura, M. E.; Nicklass, A.; Palmieri, P.; Pitzer, R.; Schumann, U.; Stoll, H.; Stone, A. J.; Tarroni, R.; Thorsteinsson, T. MOLPRO, version 2006.1, a package of ab initio programs; see http://www.molpro.net.

(30) Knowles, P. J.; Hampel, C.; Werner, H.-J. *J. Chem. Phys.* **1993**, *99*, 5219. (a) Erratum: *J. Chem. Phys.* **2000**, *112*, 3106.

(31) Kendall, R. A., Jr.; Harrison, R. J. *J. Chem. Phys.* **1992**, *96*, 6796.

(32) Peterson, K. A. Private communication (July 10, 2008).

(33) Dunning, T. H., Jr.; Peterson, K. A.; Wilson, A. K. *J. Chem. Phys.* **2001**, *114*, 9244.

(34) Helgaker, T.; Klopper, W.; Koch, H.; Noga, J. *J. Chem. Phys.* **1997**, *106*, 9639.

(35) Peterson, K. A., Jr *J. Chem. Phys.* **2002**, *117*, 10548.

(36) de Jong, W. A.; Harrison, R. J.; Dixon, D. A. *J. Chem. Phys.* **2001**, *114*, 48.

(37) Feller, D. *J. Comput. Chem.* **1996**, *17*, 1571.

(38) Schuchardt, K. L.; Didier, B. T.; Elsethagen, T.; Sun, L.; Gurumoorthi, V.; Chase, J.; Li, J.; Windus, T. L. *J. Chem. Inf. Model* **2007**, *47*, 1045.

(39) Dribinski, V.; Ossadtchi, A.; Mandelshtam, V. A.; Reisler, H. *Rev. Sci. Instrum.* **2002**, *73*, 2634.

(40) Liyanage, R.; Yang, Y. A.; Hashimoto, S.; Gordon, R. J.; Field, R. W. *J. Chem. Phys.* **1995**, *103*, 6811.

(41) Rakitzis, T. P.; Zare, R. N. *J. Chem. Phys.* **1999**, *110*, 3341.

(42) Rakitzis, T. P.; Kandel, S. A.; Alexander, A. J.; Kim, Z. H.; Zare, R. N. *J. Chem. Phys.* **1999**, *110*, 3351.

(43) Samartzis, P. C.; Bakker, B. L. G.; Rakitzis, P.; Parker, D. H.; Kitsopoulos, T. N. *J. Chem. Phys.* **1999**, *110*, 5201.

(44) Bass, M. J.; Brouard, M.; Clark, A. P.; Vallance, C.; Martinez, Haya. *Phys. Chem. Chem. Phys.* **2003**, *5*, 856.

(45) From the excited-state geometry reported by Martin et al.,[4] we calculate an impact parameter of 0.43 Å. Using an impulsive model, radicals formed with $E_T = 25$ kcal/mol have 13 kcal/mol imparted to rotational energy.

(46) Baboul, A. G.; Curtiss, L. A.; Redfern, P. C.; Raghavachari, K. *J. Chem. Phys.* **1999**, *110*, 7650.

JP8057417